Solar Array Operation in HCT Plume: Electrostatic Discharge Generated Plasma Expansion Velocity Measurements

IEPC-2013-316

Presented at the 33rd International Electric Propulsion Conference,
The George Washington University • Washington, D.C. • USA
October 6 – 10, 2013

Justin J. Likar[1], Robert E. Lombardi[2], and Kevin August[3]
Lockheed Martin Space Systems, Newtown, PA, 18940, USA

Yevgeny Raitses[4], Abraham Chien[5], Martin Griswold[6]
Princeton Plasma Physics Laboratory, Princeton, NJ, 08543, USA

Keith Kannenberg[7]
Lockheed Martin Space Systems, Sunnyvale, CA, 94089, USA

and

Brian Jones[8]
Lockheed Martin Advanced Technology Center, Palo Alto, CA, 94304, USA

The total plasma environment that surrounds operating spacecraft includes, in addition to the ambient plasma, the dynamic plasma generated by spacecraft electric propulsion system. Geostationary Earth Orbiting spacecraft solar arrays operating in the presence of a Hall Current Thruster plume are subjected to plasma conditions similar to, or more severe than, those present at Low Earth Orbit where plasma conditions support the susceptibility of electrostatic discharge events, or arcs, on the spacecraft surface. During spacecraft electrostatic discharge events, the return current waveform depends on how rapidly and completely spacecraft dielectric surfaces are discharged by the plasma created by the ESD event as it expands outward, rendering the expansion velocity a critical parameter of interest. The velocity of arc-produced plasma was measured in the LEO-like plume plasma present in the backflow region of an operating 3 cm diameter 300 W cylindrical Hall thruster operating on Xenon gas. Distributed LPs were used in detecting and measuring arc-generated plasma signals, and ultimately in deriving the plasma velocity normal to the test article and horizontal to the test article (across the surface). Primary arc inception thresholds measured on a small number of large area solar cells in a representative Xenon plasma of density revealed a susceptibility at -100 V or below. The occurrence of primary arcs at such bias levels is of critical design importance for spacecraft where spacecraft floating potential approaches this value during HCT operation or at thruster startup.

[1] Staff Systems Engineer and Associate Manager, Specialty Engineering, justin.j.likar@lmco.com.
[2] Senior Systems Engineer, Specialty Engineering, robert.lombardi@lmco.com.
[3] Senior Systems Engineer, Specialty Engineering, kevin.august@lmco.com.
[4] Principal Research Physicist, Princeton Plasma Physics Laboratory, yraitses@pppl.gov.
[5] Princeton Plasma Physics Laboratory, achien@princeton.edu.
[6] Princeton Plasma Physics Laboratory, mgriswold@pppl.gov.
[7] Staff Aeronautical Engineer, Flight Sciences Engineering, keith.kannenberg@lmco.com.
[8] Senior Staff Research Scientist, Thermal and Energy Sciences, brian.b.jones@lmco.com.

Nomenclature

E_{ion} = Plasma ion energy (eV)
C_s = Speed of sound (m/s)
e = Electron charge
ϕ_f = Plasma potential (V)
h_s = Plasma sheath thickness (m)
i_{SAT} = Langmuir probe saturation current (A)
k_B = Boltzmann constant (8.62×10^{-5} eV/K)
l = Langmuir probe length (m)
λ_D = Debye length (m)
M = Molar Mass (g/mol)
N_A = Avogadro constant (6.02×10^{23} mol^{-1})
n = Density of ions, general type (m^{-3})
$\bar{n}$ = Plasma bunch number density (m^{-3})
n_p = Plasma number density (m^{-3})
n_{PLA} = Aluminum plasma number density at LP (m^{-3})
n_{SS} = Plasma number density of Solid State aluminum (m^{-3})
R_p = Langmuir probe radius (m)
ρ = Mass density (kg/m^3)
S = Langmuir probe surface area (m^2)
T_e = Electron plasma temperature (eV)
U = Characteristic plasma bunch velocity (m/s)
u = Local plasma flow velocity (m/s)
V_B = Bohm velocity (m/s)
V_H = Arc plasma expansion velocity horizontally or parallel to coupon surface (m/s)
V_N = Arc plasma expansion velocity normal to coupon surface (m/s)
$\bar{x}$ = Position of plasma bunch (m)

I. Introduction

Electrostatic Discharges (ESD) on spacecraft may result in power system disruptions, operational mode changes, non-catastrophic but degraded solar cell performance, or permanent failure of solar array circuits. Modern spacecraft manufacturers often conclude that the complete or total prevention of ESD is impractical due to cost, mass, complexity, or schedule impacts and opt instead in favor to design against the results of ESD. In doing so the energies and currents involved in ESD are of great concern, and understanding the manner with which the expanding plasma discharges the spacecraft becomes an important goal. One of the most important, yet most poorly known quantities in determining ESD currents for spacecraft arcing events is the plasma propagation speed [1].

In a dense plasma, such as that in Low Earth Orbit (LEO), dielectric surfaces can be discharged by the ambient plasma because of the change of surface potentials due to capacitive coupling with the underlying conductor connected to the arc-site. A typical ESD event on a spacecraft solar array is triggered by a blowoff discharge attributed to the spacecraft capacitance. The blowoff discharge leads to flashover discharge on the solar array surface, the energy source of which is the capacitance of the solar cell cover glass (CG) and the dielectric solar panel substrate (surface onto which the cells are bonded). Because the spacecraft capacitance (typically on the order of ~nF) is less than the capacitance of the coverglass and substrate surface (typically on the order of μF for designs which do not include conductive coatings on the CG), flashover discharge is the major current contributor to ESD energy.

It has been shown previously [2] that all electrically-connected surfaces will discharge to a high degree whether or not the expanding arc plasma reaches the surfaces. In such cases current consists of flashover current [3-5] as well as ambient collection currents, which, depending on ambient plasma density, can be the significant contributor to surface discharge. A complete physical understanding of flashover pulse formation and propagation is required as practical limitations necessitate that grounding testing is performed on small solar array coupons (sizes <1 m^2) rather than on large flight-like production solar panels (sizes >10 m^2) wherefore it is necessary to electrically simulate the full flashover current pulse. Recent attempts to characterize expansion velocity on an array in LEO plasma were met with limited success [6].

When an ESD event occurs in GEO, the return current waveform depends on how rapidly and completely spacecraft dielectric surfaces are discharged by the plasma created by the ESD event as it expands outward. The ESD current in this case, except for a brief blowoff current to discharge the spacecraft capacitance to space, consists entirely of flashover current; it is the rate of discharge of spacecraft surfaces that determines this current and several physical possibilities exist. If the expanding plasma completely discharges all dielectrics, all of the spacecraft surface capacitances will add to the total discharge current and energy. However, if the expanding plasma discharges surfaces slowly and incompletely, the currents will be less and the total energy released will be less. Finally, if the ESD arc-current stops before all the surfaces are discharged, the total discharge energy will be significantly reduced. Thus, the expansion rate of the flashover plasma and the degree to which it discharges surfaces can mean the difference between a rapid, high current event, which may lead to power system disruptions, single event upsets, damaged solar cells, or even a sustained discharge on solar array surfaces or a slow, low current event, which leads to no disruptions or damage [1].

Published experimental results identify an expansion velocity within the range of 7 km/s to 140 km/s with most falling between 10 km/s and 30 km/s [1].

Plasma conditions which enable ESD on operating solar arrays are not limited to LEO. Spacecraft solar arrays operating in the presence of a Hall Current Thruster (HCT) plume are subjected to plasma conditions similar to, or more severe than, those present at LEO [7]. The total plasma environment includes plasma generated by spacecraft electric propulsion (arcjets, Hall thrusters, and Ion thrusters) and possibly other sources. This was shown to be a critical consideration because when thrusters are fired they can surround GEO spacecraft with LEO-type plasma; consider plasma densities in the ionospheric F2 layer of 10^5 cm^{-3} to 10^6 cm^{-3} [8]. Understanding interactions with such a plasma in all spacecraft operating modes is paramount when designing GEO solar arrays. It is especially important if thrusters are fired during the time a spacecraft is negatively charged by GEO plasma as interactions may result in unexpected synergistic effects that can lead to ESD events and damage of solar arrays [9].

Although the accommodation of HCT, and similar advanced EP systems, on spacecraft presents numerous design challenges, including surface coating / film erosion, surface contamination, current collection by exposed metals / conductors, spacecraft floating potential variations, electromagnetic interference, plume-induced torques, and so on, the present study addresses electrostatic discharges induced by the high density plasma plume.

A number of public and proprietary tools are available to characterize various aspects of the plume environment in the presence of a spacecraft. It is not trivial to extend ground-based plume property characterization to flight-like or on-orbit systems and there are few examples of high quality sensors or sensor suites operating on spacecraft which utilize HCTs. Certainly defining an appropriate plume environment at the spacecraft solar array surfaces will be mission / spacecraft specific and depending upon many variables. However, present best efforts yield predicted plume plasma densities at solar array surfaces in the range of 10^{12} m^{-3} to $>10^{14}$ m^{-3} using tools developed by [10, 11]. Predicted ion energies are typically <80 eV although in some specific system architectures, thruster operating modes, and solar array configurations portions of the array surfaces may see ions of energy >120 eV.

An operating HCT will affect the spacecraft floating potential, or the potential at which the spacecraft single point ground sits relative to the surrounding plasma environment. The spacecraft potential is a dynamic, equilibrium value, resulting from current balance to exterior spacecraft surfaces; the net sum of currents to spacecraft surfaces must be zero. Positively charged surfaces readily attract electrons whilst negatively charged surfaces attract ions. Spacecraft design features which have a profound impact on spacecraft floating potential include grounding methods of the spacecraft Electrical Power System (EPS) and solar arrays, bus voltage, grounding methods of the spacecraft Electric Propulsion system (Hall Current Thruster for example), and selection of exterior materials which include properties such as surface resistivity, bulk resistivity, Secondary Electron Emission (SEE) coefficients, and photoelectric emission coefficients. It is expected that the floating potential of a typical 70 V or 100 V spacecraft will float a few volts negative and within a few volts of the negative spacecraft bus voltage during HCT operation [12, 13]. The ultimate design and operational impacts of this value can be profound as an operating solar array will float to the same value during thruster firings and modern solar cells have been demonstrated to be susceptible to electrostatic discharges at values less than -100 V [14].

The purpose of present study is to:

1. Expand the, presently, limited set of data available on the primary arc inception voltage threshold for modern large area (~60 cm^2) solar cells exposed to a simulated HCT environment.
2. Perform empirical measurements of the arc-generated plasma propagation speed in the presence of a simulated spacecraft solar panel.

II. Primary Arc Inception

A low primary arc inception threshold that is less than, or near, the spacecraft floating potential in high density plasma means that frequent ESD may occur on the operating solar array. Recently, attention has been paid to the cumulative operational effects of repeated low power Primary Arcing (PA). Round Robin testing had been previously performed at a number of ground test laboratories on a standard selection of Silicon and Multi-Junction (MJ) GaAs space solar cells per methodology summarized in the ISO Standard for ESD Testing of Space Solar Arrays (ISO-CD-11221). Ground test results to date have been quite informative suggesting that advanced technology cells, which employ more junctions, are more susceptible to the degrading effects of primary arcs at the cell perimeter. Such testing and related analytical studies have provided insight into potential mechanisms for PA induced cell degradation while also parameterizing some effects as a function of PA energy, number, and cell type. Further, an increased likelihood of primary arc necessarily increases the potential for more damaging secondary arcs.

Two coupons were studied. Both included a 2 mil (0.05 mm) Kapton® substrate and large area solar cells. One coupon contained 8 Emcore ZTJ solar cells arranged to form 2 strings of 4 cells; the second coupon contained 8 Spectrolab XTJ solar cells arranged to form 2 strings of 4 cells. The XTJ cells include an area of 59.65 cm^2, an Open Circuit Voltage (V_{OC}) of 2.63 V, and a Short Circuit Current (I_{SC}) of 17.76 mA/cm^2 or 1.06 A. The ZTJ cells include an area of 59.3 cm^2, V_{OC} of 2.72 V, and I_{SC} of 17.4 mA/cm^2 or 1.03 A.

Testing was performed in the Lockheed Martin Advanced Technology Center (ATC) Spacecraft Charging Test Facility in Palo Alto, CA. The vacuum chamber used in testing has an internal diameter of approximately 1.2 m, and an internal length of approximately 1.8 m. Two solar array test coupons were mounted, independently, on nylon standoffs, electrically isolated from the chamber. A single, planar, Langmuir probe was mounted on a horizontal trolley, permitting plasma density measurements to be taken at various points across the sample surface. A Faraday cup and a conducting plate were installed adjacent to the sample to measure plasma current. All bus bars (turnarounds) were encapsulated / covered with Kapton® tape to ensure all discharges occur at solar cell edges.

The HCT plume was simulated with a mono-energetic Xenon plasma was generated using a 3 cm diameter Commonwealth Scientific Corporation Ion Source with Graphite Collimated Ion Optics and an IBS 250 power supply (shown in Fig. 1). The source was originally designed for sputtering applications however, with ion energy reduced to a minimum value (<50 eV) and the source located placed ~50 cm away from the coupon, a broader plasma was created purposes of

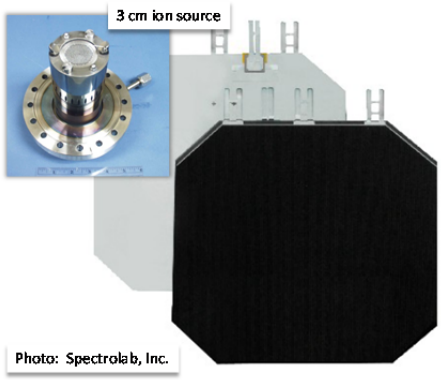

Figure 1. Solar cell and ion source used in primary arc inception threshold measurements. *Cells arranged in 2 strings adhered to a dielectric (Kapton®) ~0.1 m^2 substrate. Cell photo credit: Spectrolab, Inc. (www.spectrolab.com).*

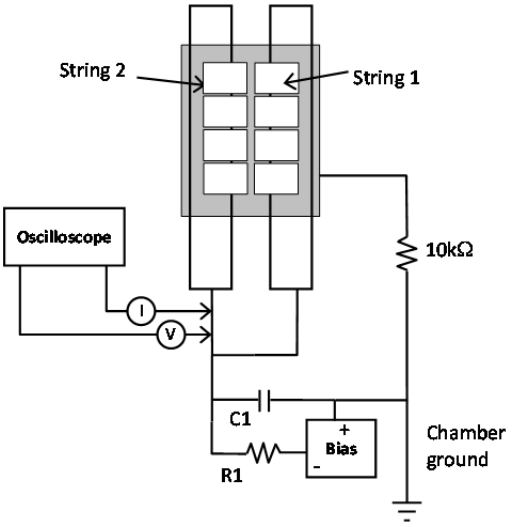

Figure 2. Electrical circuit used for primary arc inception measurements. *Value of R1 is 10 kΩ; value of C1 is 0.066 μF.*

simulating the environment predicted at a solar array surface operating in an HCT plume.

LP measurements made at several locations across the sample surface confirmed a peak plasma density of 2×10^8 cm^{-3} with an ion energy of <50 eV. A DC bias was applied to the LP to ensure that ion saturation current was reached in the presence of the 50 eV xenon ions.

The intent of testing was to establish the primary arc inception threshold of the coupon design described above. Electrostatic discharges were detected using an RF antenna installed inside the vacuum chamber.

In performing characterization of the primary arc threshold the ends of each string are electrically shorted together and the string (or strings) biased to the desired negative voltage with an external DC power supply as shown Fig. 2. The selected electrical circuit includes a large resistor, which limits current from the power supply. Negative DC bias was swept from -70 V to -300 V in 25 V increments with a dwell time that did not exceed 20 min. Arcs were observed at several voltages with a threshold limit of -100 V for both XTJ and ZTJ cell types. It is noteworthy that these levels are below those reported for identical cell types in a simulated (less dense) Arcjet plume plasma [14].

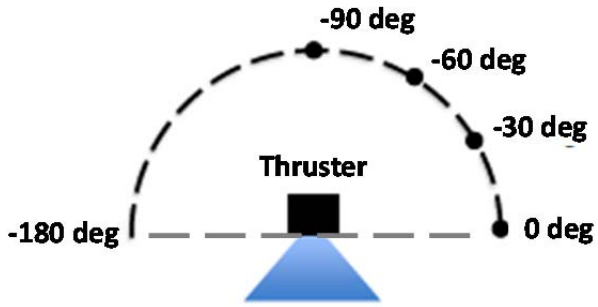

Figure 4. Plume plasma characterization behind thruster. *Langmuir probe was swept through region behind thruster at fixed distance of 72 cm from thruster exit plane; no panel surface present during measurement.*

III. Plasma Expansion Velocity

Evidence of the HCT plume plasma similarities with LEO is demonstrated by compliance with test conditions needed to study the expansion velocity of an ESD-generated plasma in accordance with the on-going AFRL Round-Robin test program [1]. In supporting the on-going Round-Robin test program, the present test utilizes a simplified solar array test article and test schematic / circuit [1]. It is intended for arcs to initiate at a single site and for the arc plasma to expand symmetrically about this point.

All testing was performed in the 8.4 m × 2.2 m Hall Thruster Experiment (HTX) vacuum vessel located at Princeton Plasma Physics Laboratory (PPPL) in Princeton, New Jersey. Arcs are generated by biasing the test article in the back flow region of a Cylindrical Hall Thruster (CHT) operating at PPPL and shown in Fig. 3. The plasma properties represent realistic conditions to which an operating solar array will be subjected during typical mission; with an average density of 1.5×10^6 cm^{-3} and temperature of 2.5 eV, they also represent, quite well, LEO plasma conditions. ESD-generated plasma is measured with Langmuir probes at points ~10 cm directly above every test article segment and m directly above the arc-site.

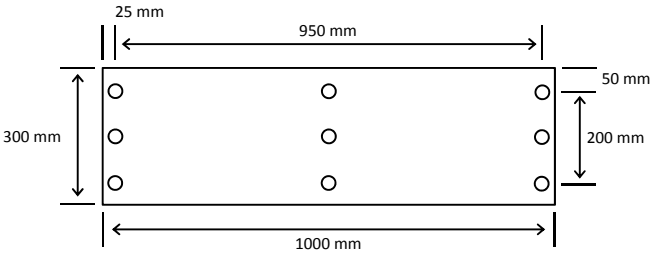

Figure 5. Plume plasma characterization on simulated solar panel surface behind thruster. *Nine surface mounted LPs were used to characterize plume plasma at the surface of a simulated solar panel.*

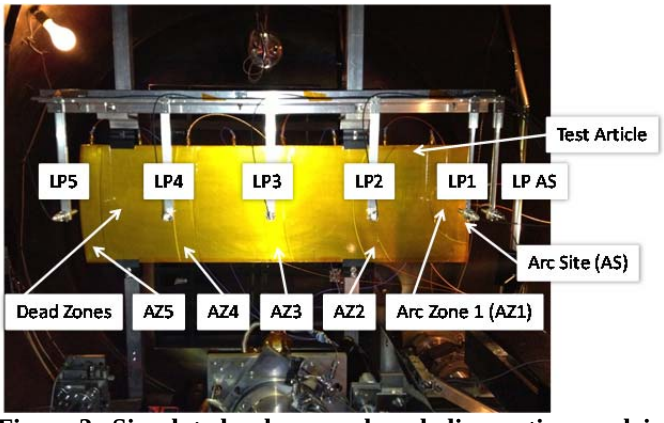

Figure 3. Simulated solar panel and diagnostics used in plasma expansion velocity measurements. *The simulated solar panel and diagnostics were installed in backflow region (behind) the Cylindrical Hall Thruster (shown but not annotated) visible in lower middle portion of photo.*

A. Background Plasma Characterization

Desired plasma conditions include background pressure $<10^{-5}$ torr, plasma density (n_p) ~10^6 cm^{-3}, electron temperature (T_e) <5 eV, and ion energy (E_{ion}) <5 eV.

Thruster operational parameters include discharge voltage of 250 V; discharge current of

0.79 A; power of 197.5 W; cusp magnetic field of +2.5 A (BC) and -1.0 A (FC); and xenon flow rate of 4 sccm (anode) and 2 sccm (cathode). In all cases the chamber pressure with thruster operating was $<1.6\times10^{-6}$ torr.

Position of the test coupon was determined by characterizing the background plasma behind the operating thruster. As shown in Fig. 4 a Langmuir Probe was swept, at a fixed distance of 72 cm from the thruster exit plane from a position parallel with the exit plane (0 deg), to directly behind the thruster, to a cylindrically symmetric position directly parallel with the thruster exit plan on the opposite side (-180 deg) while characterizing the plasma at several intermediate locations (-30 deg, -60 deg, and -90 deg). Measurements demonstrated that plasma density is quite uniform behind the thruster (angles between approximately -30 deg and -150 deg).

Results of this initial characterization yield T_e of <3.5 eV, n_p between 2×10^6 cm^{-3} and 3×10^6 cm^{-3}, E_{ion} of <5 eV, and ϕ_f of +0.6 V suggesting plasma conditions are satisfactory to simulate LEO environment as desired for Round Robin testing.

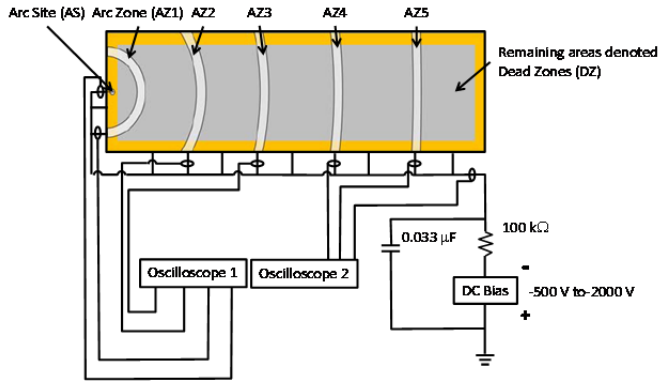

Figure 6. Electrical schematic used in plasma expansion velocity measurements. *Resistor and capacitor values as noted; LP acquisition triggered from CP oscilloscope. Arc Site shown at left in figure.*

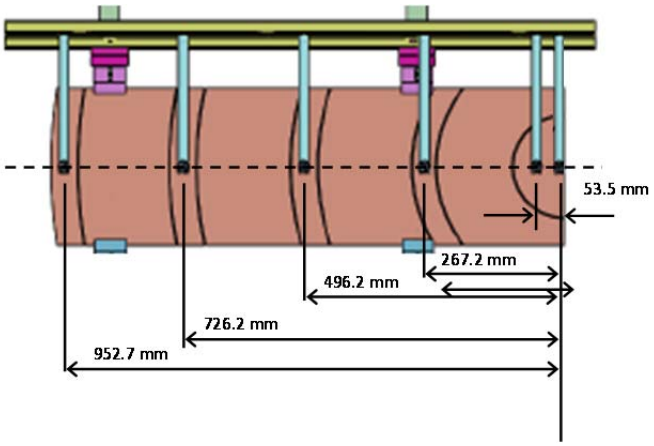

Figure 7. LP locations on simulated solar panel. *LPs denoted (from right-to-left) as LP_{AS} (Arc Site), LP_1, LP_2, LP_3, LP_4, and LP_5.*

B. Plasma Characterization at Surface of Simulated Solar Panel

Plume plasma was characterized on the surface of a simulated Round Robin test coupon using a machined flat aluminum plate of dimensions equal to the Round Robin coupon (30 cm × 100 cm) and thickness of 0.25 in (0.635 cm).

An array of 9 planar geometry probes was flash-mounted to the coupon surface as shown in Fig. 5. The probe radius (R_p) was 1.25 cm, and for a plasma density on the order of 10^6 cm^{-3} and electron temperature of 2.5 eV, the Debye length (λ_D) is approximately 1 cm. When the characteristic dimensions of $R_p \approx \lambda_D$ the planar probe operates much like a spherical probe.

Thruster operating parameters were identical to those noted in the previous section with exception of slightly lower discharge current (0.7 A) and higher power (175 W). Measurement results indicate an average plasma density of 1.5×10^6 cm^{-3} with a deviation from average that does not exceed ±20% at any of the 9 probe positions.

C. Characterization of Electrostatic Discharge Generated Plasma Expansion Velocity

The Round Robin test coupon was installed behind the thruster as shown in Fig. 3.

Supplied by AFRL KAFB the test coupon was a long (100 cm × 30 cm) aluminum panel segmented as shown in Fig. 6 and Fig. 7 and covered with a 1 mil (0.0254 mm) layer of Kapton® HN. This construction enables simulation of the capacitance per unit area of a solar array [4]. Segments of the test coupon were electrically connected with wires (see schematic in Fig. 6) but insulated from each other in every other way. Wires to certain segments, denoted Arc Zone 1 through Arc Zone 5), included electrometers (Pearson coils) on lines connecting them to all other segments, so currents to or from these segments can be measured. All aluminum segments were biased (DC) by a power supply to the same negative bias, simulating an inverted gradient condition on a spacecraft solar array. All edges and back of the coupon were covered with Kapton® tape with the exception of a small area, denoted "Arc Site" where the metal-Kapton® boundary was left uncovered. It was intended, by design [1], for arcs to occur at this site and for the arc plasma to expand symmetrically about this point.

Six cylindrical Langmuir Probes were installed a fixed distance (10 cm) from the coupon surface for purposes of characterizing expansion plasma properties. Each probe was 0.96 cm in diameter and 2 cm in length. Specific probe locations are defined by [1] and noted in Fig. 7. Each probe is biased relative to ground via a 1 kΩ resistor place immediately adjacent to the probe (interior to chamber). Voltage measured across the resistor yields current collected by the probe. Coaxial cabling was used for all probe wiring.

The test coupon was designed to enable all segments and the arc site to be biased to negative potentials (between -500 V and -1500 V) uniformly / simultaneously; such values are comfortably below the breakdown strength of 2 mil Kapton® HN. Shown in Fig. 6, the bias circuit included a 100 kΩ resistor in series and a 0.033 μF capacitor in parallel so as to decouple the discharge event from the bias power supply over the entire timescale of the ESD event but not contribute significant capacitive energy to the discharge, compared with the capacitance of the sample. The bias circuit is similar to that used for primary arc threshold determination, described in Section II.

Care was used to minimize, where possible, cable lengths on all harnesses; where not possible to minimize cable length care was taken to ensure equal length, and identical type cables. Insulated 8 ft (2.44 m) wires were used to make all connections with the test coupon; male banana plugs were overwrapped with Kapton® tape to ensure no exposed metal. The same cables connected to N-type chamber feedhtroughs via a BNC-to-N-type adapters. On the chamber exterior 15 ft (4.57 m) RG58 coaxial cables were used for interface between chamber and the breakout box (coil box). The same length / type cables were used for the breakout box to RC circuit interface. 3 ft (0.91 m) RG58 coaxial cables were used to connect to 2 Tektronix DPO4104B oscilloscopes (1 GHz bandwidth and 5 GS/s rate), used to monitor and record transients, via computer, on the current probes. All data collection was triggered either by the detection of arc either by current probe (CP) or high voltage (HV) probe (not shown) placed on the Arc Site line; delay between Oscilloscope 1 and Oscilloscope 2 was measured at ~30 ns. Approximately the same delay was measured between Oscilloscope 1 and the multiple oscilloscopes used to record LP data, which were also triggered in the same manner.

In accordance with the spirit of Round Robin agreements we present only analysis of LP arc generated plasma measurements. Additional analyses complete with CP measurements, neutralization current studies, et cetera to be published with Round Robin co-authors.

It can be shown that the amount of aluminum material ablated or evaporated during the electrostatic discharge event is sufficient to enable detection at the Langmuir Probes ≥10 cm from the arc site. Assuming a realistic arc site diameter of 1 μm the number density of aluminum at the arc site is calculated as,

$$n_{ss} = \frac{\rho}{M}(N_A) = 6.022 \times 10^{28} m^{-3}, \qquad (1)$$

which can be scaled as $\sim r^{-2}$, assuming radial expansion, yielding a scaled number density of aluminum at the Langmuir probe (n_{LPA}) of 6.02×10^{18} m^{-3}. Given that this value is larger than the, soon to be discussed, empirically measured plasma density of $\sim10^{17}$ m^{-3} on LP_1 (10 cm directly above the arc site) one may conclude that there is sufficient aluminum ablated during the arc to form the entirety of the measured arc plasma.

Assumptions made when analyzing the LP data include assertions that arc-generated plasma is single species and quasi-neutral of constant electron temperature [15]. Further, the authors assume that nearest LPs do not shadow those measurements at farther LPs and that there is no secondary electron emission from the probe surfaces [15].

Density at the Langmuir Probes was obtained starting with the classical expression for saturation current for a cylindrical probe,

$$i_{SAT}(t) = \frac{\sqrt{2}}{\hat{e}} S(t) e n(t) V_B = \frac{V(t)}{R} \qquad (2)$$

where Bohm velocity (V_B),

$$V_B = \sqrt{k_B T_e / M}, \qquad (3)$$

is replaced by the average measured horizontal plasma expansion velocity as this value exceeds the Bohm velocity. The calculation includes probe surface area,

$$S(t) = 2\pi\big(r + h_S(t)\big)l, \qquad (4)$$

with parameters as noted above, sheath thickness [15],

$$h_s(t) = \sqrt{\frac{4\hat{e}}{9}}\left(\frac{eV(t)}{k_B T_e}\right)^{3/4} \lambda_D(t), \quad (5)$$

and Debye length,

$$\lambda_D(t) = \left(\frac{k_B T_e}{4\pi e^2 n(t)}\right)^{1/2}, \quad (6)$$

Combining all formulas one obtains density as a function of time, plotted in Fig. 8. One immediately recognizes peak density at LP_{AS} (Arc Site) of ~10^{17} m^{-3} and for background (with thruster operating) ~10^{12} m^{-3} although not discernible by axes on this plot. It is recognized that maximum sheath size ($h_S(t)$) is small (0.1 cm) compared to probe radius (~0.5 cm).

During multiple days of testing more than 50 arcs were generated at sample bias voltages between -500 V and -1500 V DC. Fig. 9 includes a sample of the LP traces acquired for one arc; LP and CP responses were, as expected, quite repeatable wherefore data plotted in Fig 9 should be considered typical. Note that "LP Arc" annotation corresponds to LP located directly above Arc Site and LP_1 corresponds to LP directly above Arc Zone 1 (AZ1). The sign of LP current corresponds to probe operating in ion collecting mode. The unmistakable observation of two prominent peaks of same polarity, on both probes, may be indicative of the existence of two plasma "bunches" arriving at each LP with delay of a few milliseconds. Making the assumption that all plasma "bunches" propagate with the same velocity then time separation and velocity average over all shots yield values of

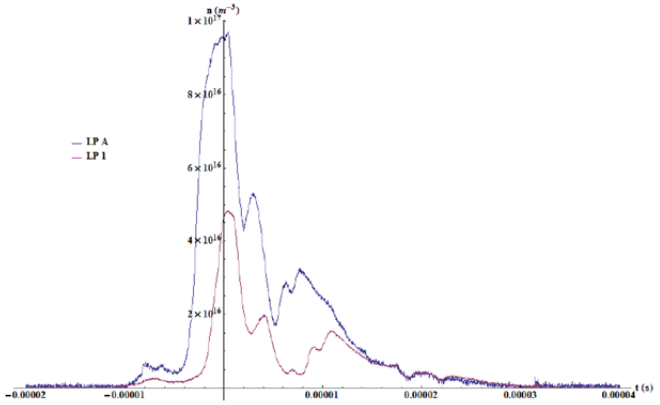

Figure 8. Arc-generated plasma density as function of time. *Sign of the LP current indicates operation in ion collecting mode; multiple peaks may indicate multiple plasma "bunches" arriving over several ms.*

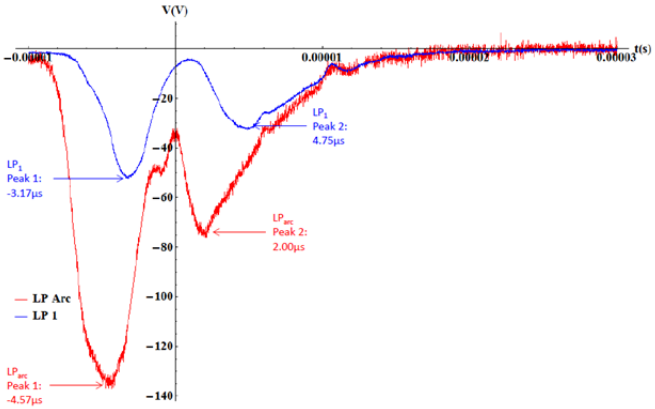

Figure 9. Captured Langmuir probe traces during arc generated plasma event. *Sign of the LP current indicates operation in ion collecting mode; multiple peaks may indicate multiple plasma "bunches" arriving over several ms.*

$$\Delta t = (1.69 \pm 0.89) \times 10^{-6}\ s \quad (7)$$

and

$$v = (3.17 \pm 1.6) \times 10^{4}\ m/s \quad (8)$$

If one treats each plasma "bunch" independently then time separation and velocity average over all shots yields

$$\Delta t_1 = (1.57 \pm 0.19) \times 10^{-6}\ s$$
$$\Delta t_2 = (2.79 \pm 0.17) \times 10^{-6}\ s \quad (9)$$

and

$$v_1 = (3.41 \pm 0.41) \times 10^{4}\ m/s$$
$$v_2 = (1.92 \pm 0.12) \times 10^{4}\ m/s \quad (10)$$

The values are within the accepted range published by spacecraft charging community [1] as well as within 2× of values published by [15] and [16].

Physically one expects that Current Sensors to see a signal before the LPs. The vertical velocity, or arc-generated plasma velocity normal to the coupon surface, can be obtained by measuring the time difference between CP and LP signals corrected for signal delays in cables. Assuming, again, independent plasma "bunches" as above, we find,

$$\Delta t_1 = (6.88 \pm 0.93) \times 10^{-6}\ s$$
$$\Delta t_2 = (1.56 \pm 1.12) \times 10^{-6}\ s \qquad (11)$$

and

$$v_1 = (1.45 \pm 0.20) \times 10^4\ m/s$$
$$v_2 = (6.60 \pm 4.11) \times 10^4\ m/s \qquad (12)$$

Plasma expansion may also be studied by, again, referring to Fig. 8 which plots density as function of time for both LPs above the Arc Site and Arc Zone; distance from arc source (Arc Site) and LP_1 is $\sqrt{(10\ cm)^2 + (5.35\ cm)^2}$ or 11.34 cm. Assuming radial, isothermal expansion slope should be equal to ratio of squared radius $11.34^2/10^2 = 1.29$ or $\rho_{AS} \approx 1.29\ \rho_{AZ1}$. If one assumes adiabatic expansion, and not isothermal expansion [17], ion density may be scaled with time and position as,

$$n(x,t) = \frac{n_0}{\sqrt{1+\Omega^2 t^2}} N\left(\frac{x}{\sqrt{1+\Omega^2 t^2}}\right)\ , \qquad (13)$$

where

$$N(U) = exp\left(-\frac{U^2}{2C_S^2}\right). \qquad (14)$$

[17] gives the velocity profile with time and position as,

$$u(x,t) = \frac{xt\Omega^2}{1+\Omega^2 t^2}\ . \qquad (15)$$

Switching into the reference frame of the expanding plasma pulse ("bunch") the density scaling can be expressed as a function of time only,

$$\bar{x}(t) = \bar{x}(0)\sqrt{1+\Omega^2 t^2}, \qquad (16)$$

where $\bar{x}(t)$ represents the position of the plasma "bunch" at time *t* based on integrating the velocity profile. This enables computation of $\bar{n}(t) = n(\bar{x}(t), t)$ where n_0 is an arbitrarily chosen density of 1.0 at the location of the Arc Site LP. When time (*t*) is 2 μs, which corresponds to plasma arrival at LP1, one obtains a theoretical ratio of $\rho_{AS} \approx 1.39\ \rho_{AZ1}$. This ratio can be compared to same ratio as obtained from strictly a statistical review of empirical data ($\rho_{AS} \approx 2.08\ \rho_{AZ1}$) and an assumed isothermal expansion, as described above ($\rho_{AS} \approx 1.29\ \rho_{AZ1}$). We recognize that, instead of scaling as r^{-2} density scales as a higher power of *r* and plasma density decreases more quickly than predicted.

IV. Conclusion

The velocity of arc-produced plasma was measured in the LEO-like plume plasma present in the backflow region of an operating 3 cm diameter 300 W cylindrical Hall thruster operating on Xenon gas. Backscattering and charge exchange collisions in the Xenon thruster plume produce background plasma in the vacuum vessel, including at the test article placement. Repeated Langmuir Probe measurements characterized the plume plasma in the backflow region in an empty vacuum chamber and on the surface of a simulated solar array panel. Distributed LPs were used in detecting and measuring arc-generated plasma signals, and ultimately in deriving the plasma velocity normal to the test article and horizontal to the test article (across the surface):

$$v_H = (3.41 \pm 0.41) \times 10^4\ m/s$$

$v_N = (1.45 \pm 0.20) \times 10^4\ m/s.$

At 10 cm from the test cell, the arc event on the test cell causes the plasma density to increase from the background level of ~10^{12} m^{-3} to 10^{16} m^{-3} to 10^{17} m^{-3}. The observed plasma expansion cannot be explained by conventional theoretical models (isothermal and adiabatic); plasma density falls more quickly than these models predict.

Primary arc inception thresholds measured on a small number of large area solar cells in a Xenon plasma of density 10^{14} m^{-3} revealed a susceptibility at -100 V or below. The occurrence of primary arcs at such bias levels is of critical design importance for spacecraft where spacecraft floating potential approaches this value during HCT operation or at thruster startup; such spacecraft include those with operating voltages near, or above 100 V as well as spacecraft with large current collection areas.

The present test program illustrates the system-level design challenges associated with high performance HCT, and similar propulsions systems and, also, further demonstrates the utility of the PPPL HTX facility and resources for performing spacecraft charging related studies. It also illustrates the importance of understanding the spacecraft floating potential in the presence of an operating thruster that must be addressed given the recent trend in All Electric Propulsion systems. Nevertheless the goal for designers should remain the same – the optimal solution– prevent arcing on the solar array.

Acknowledgments

J. Likar is grateful to D. Ferguson and R. Hoffmann of AFRL KAFB for supplying the test article used for a portion of these experiments and for discussions on some results summarized here in which also included important contributions from B. Vayner of NASA GRC and OAI. J. Likar, Y. Raitses, M. Griswold, and A. Chien are grateful to the laboratory / test support of A. Merzhhevskiy.

References

[1]Ferguson, D., Hoffman, R., and Wheelock, A. "A U.S. Round-Robin Experiment on Plasma Propagation Velocity." 4th AIAA Atmospheric and Space Environments Conference, 2012, 10.2514/6.2012-2940.

[2]Ferguson, D., Vayner, B., Galofaro, J., and Hillard, B. "Arcing in LEO – Does the Whole Array Discharge?" 43rd AIAA Aerospace Sciences Meeting and Exhibit, 2005, 10.2514/6.2005-481.

[3]Vayner, B. "Physical Principles of Flashover Current Pulse Formation." 3rd AIAA Atmospheric Space Environments Conference, 2011, 2011, 10.2514/6.2011-3976.

[4]Okumura, T., Imaizumi, M., Nitta, K., Takahashi, M., Suzuki, T., and Toyoda, K. "Flashover Discharge on Solar Array: Analysis of Discharge Current and Image." *J. Spacecraft and Rockets*, Vol. 48, No. 2, March-April 2011, pp. 326-335.

[5]Siguier, J-M., Inguimbert, V., Sarrailh, P., Sarrail, D., Murat, G., Mateo-Valez, J-C., Payan, D., and Balcon, N. "Parametric Study of a Physical Flashover Simulator." *IEEE Trans. Nuc. Science*, Vol. 40, No. 2, February 2012, pp. 311-320.

[6]Vayner, B., Ferguson, D., Hoffmann, R., Wheelock, A., Likar, J., Prebola, J., Crider, D., Schneider, T., Vaughn, J., Hoang, B., Steele, K., Close, S., Goel, A., Crofton, M., Young, M., Bodeau, M., Noushkam, N. "Further Results from the U.S. Round-Robin Experiment on Plasma Expansion Speed." 51st AIAA Aerospace Sciences Meeting including the New Horizons Forum and Aerospace Exposition, 2013, 10.2514/6.2013-809.

[7]NASA Technical Handbook, NASA-HDBK-4002A, March 3, 2011.

[8]NASA Technical Handbook, NASA-HDBK-4006, June 3, 2007.

[9]Likar, J.,J., Bogorad, A.L., Malko, T.R., Goodzeit, N.E., Galofaro, J.T., and Mandell, M.J. "Interaction of Charged Spacecraft with Electric Propulsion Plume: On-Orbit Data and Ground Test Results." *IEEE TNS*, Vol. 53, No. 6, Part 1, 2006, pp. 3602-3606.

[10]Katz, I., Jongewrd, G., Davis, V., Mandell, M., Mikellides, I., Dressler, R., Boyd, I., Kannenberg, K., Pollard, J., and King, D. "A Hall Effect Thruster Plume Model Including Large Angle Elastic Scattering." *Presented at 37th AIAA/ASME/SAE/ASEE Joint Propulsion Conference & Exhibit*, 8-11 July 2001, Salt Lake City, Utah, USA, Paper AIAA 2001-3355.

[11]Pollard, J., Diamant, K., Khayms, V., Werthman, L., King, D., and de Grys, K. "Ion Flux, Energy, and Charge-State Measurements for the BPT-4000 Hall Thruster." *Presented at 37th AIAA/ASME/SAE/ASEE Joint Propulsion Conference & Exhibit*, 8-11 July 2001, Salt Lake City, Utah, USA, Paper AIAA 2001-3351.

[12]Estublier, D. "The SMART-1 Spacecraft Potential Investigations." *IEEE TNS*, Vol. 36, No., 5, October 2008, pp. 2262-2270.

[13]Khayms, V., Logan-Garbisch, A., and Kannenberg, K. "Measurements and Modeling of a Solar Array Floating Potential and Leakage Current in a Hall Thruster Plume Environment." *Presented at 41st AIAA/ASME/SAE/ASEE Joint Propulsion Conference & Exhibit*, 10-13 July 2005, Tucson, Arizona, USA, Paper AIAA 2005-3862.

[14]Likar, J., Okumura, T., Iwai, S., Stone, S., Gasner, S., Jenkins, P., Trautz, K., Cho, M., Lomb ardi, R., and Toyoda, K. "Initial Results from Primary Arc effects on Solar Cells At LEO (PASCAL) Flight Experiment. *Presented at 39th IEEE Photovoltaic Specialists Conference*, Tampa, Florida, 16-21 June 2013.

[15]Dunaevsky, A. and Fisch, N. "Measuring the Plasma Density of a Ferroelectric Plasma Source in an Expanding Plasma." J. Appl. Phys. Vol. 95, No. 9, February 2004, pp. 4621-4727.
[16]Gurevich, A. V. and Meshcherkin, A. P. Zh. Eksp. Theo. Fiz. Vol 53, pp. 1810.
[17]Kovalev, V., Bychenkov, Y., and Tikhonchuk, V. Zh. Eksp. Theo. Fiz. Vol 122, pp. 264.